Electronic Supplementary Material (ESI) for Journal of Materials Chemistry A.


Supporting Information for

# Ordered Mesoporous $WO_{2.83}$: Selective Reduction Synthesis, Exceptional Localized Surface Plasmon Resonance and Enhanced Hydrogen Evolution Reaction Activity†

Hefeng Cheng,[*a] Miriam Klapproth,[ab] Anton Sagaltchik[b], Shuang Li[a] and Arne Thomas[*a]

[a]Department of Chemistry, Functional Materials, Technische Universität Berlin, Hardenbergstraße 40, 10623 Berlin, Germany

[b]BasCat, UniCat BASF JointLab, Technische Universität Berlin, Hardenbergstraße 36, 10623 Berlin, Germany

## Extended Experimental Section

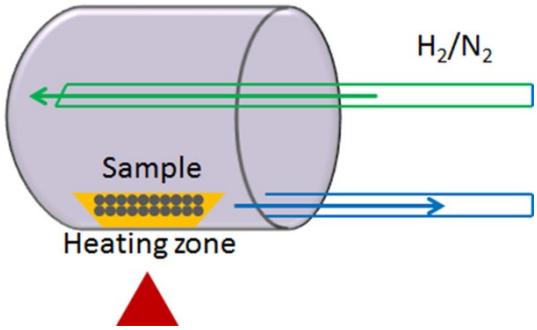


**Scheme S1.** Schematic diagram of the apparatus used for the $H_2$ reduction of the samples.

**Synthesis of Meso-$WO_3$ (AMT).** Meso-$WO_3$ (AMT) was also prepared by the nanocasting method similar to that of Meso-$WO_3$ (PTA) but with ammonium metatungstate hydrate (AMT) as precursor. Typically, 1 g of AMT was dissolved in 3 mL distilled water, and then the solution was added to the KIT-6 support by incipient wetness impregnation. The mixture was dried at 100 °C for 12 h. This impregnation process was repeated two times by adding another 3 mL of aqueous solution containing 1 g of AMT to receive a final mass ratio of 1:3 between KIT-6 support and AMT precursor. The composite was calcined at 650 °C for 4 h with a heating rate of 2 °C/min. To remove silica template, the silica/tungsten oxide composites were stirred in 100 mL of $NH_4HF_2$ (4 M) solution for 24 h, washed with water and ethanol for three times, respectively, and dried at 100 °C.

**Synthesis of mesoporous $WO_{2.83}$ (AMT).** Meso-$WO_{2.83}$ (AMT) was also obtained by $H_2$ reduction of Meso-$WO_3$ (AMT) at 550 °C for 1 h in the one-end tube furnace by the method mentioned above. The experimental parameters were kept the same.

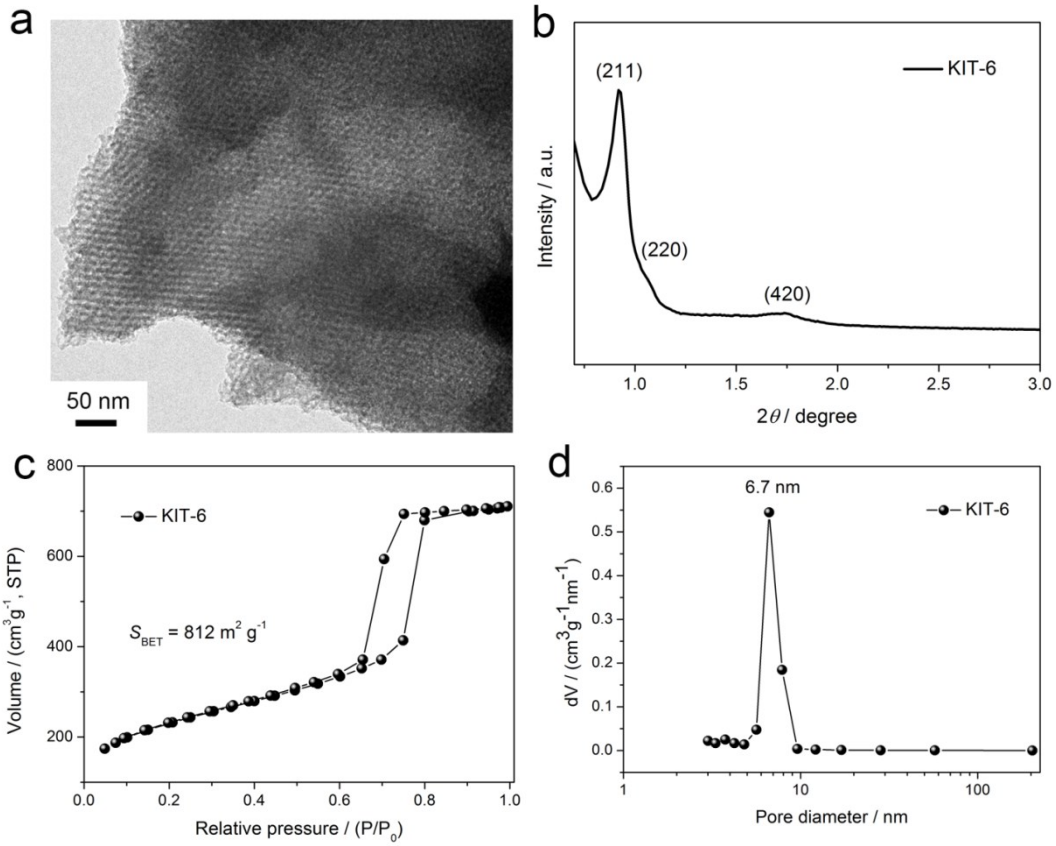


**Fig. S1** Structural characterizations of mesoporous silica (*KIT-6*). (a) Typical TEM image, (b) small-angle XRD, (c) $N_2$ sorption isotherm and (d) the corresponding pore size distribution curve of the *KIT-6* hard template. *KIT-6* possesses order mesoporous structure, and the peaks assigned to (211), (200) and (420) confirm its cubic *Ia3d* symmetry.[1] With a uniform pore size of around 6.7 nm, the *KIT-6* template has a BET surface area as high as 812 $m^2/g$.

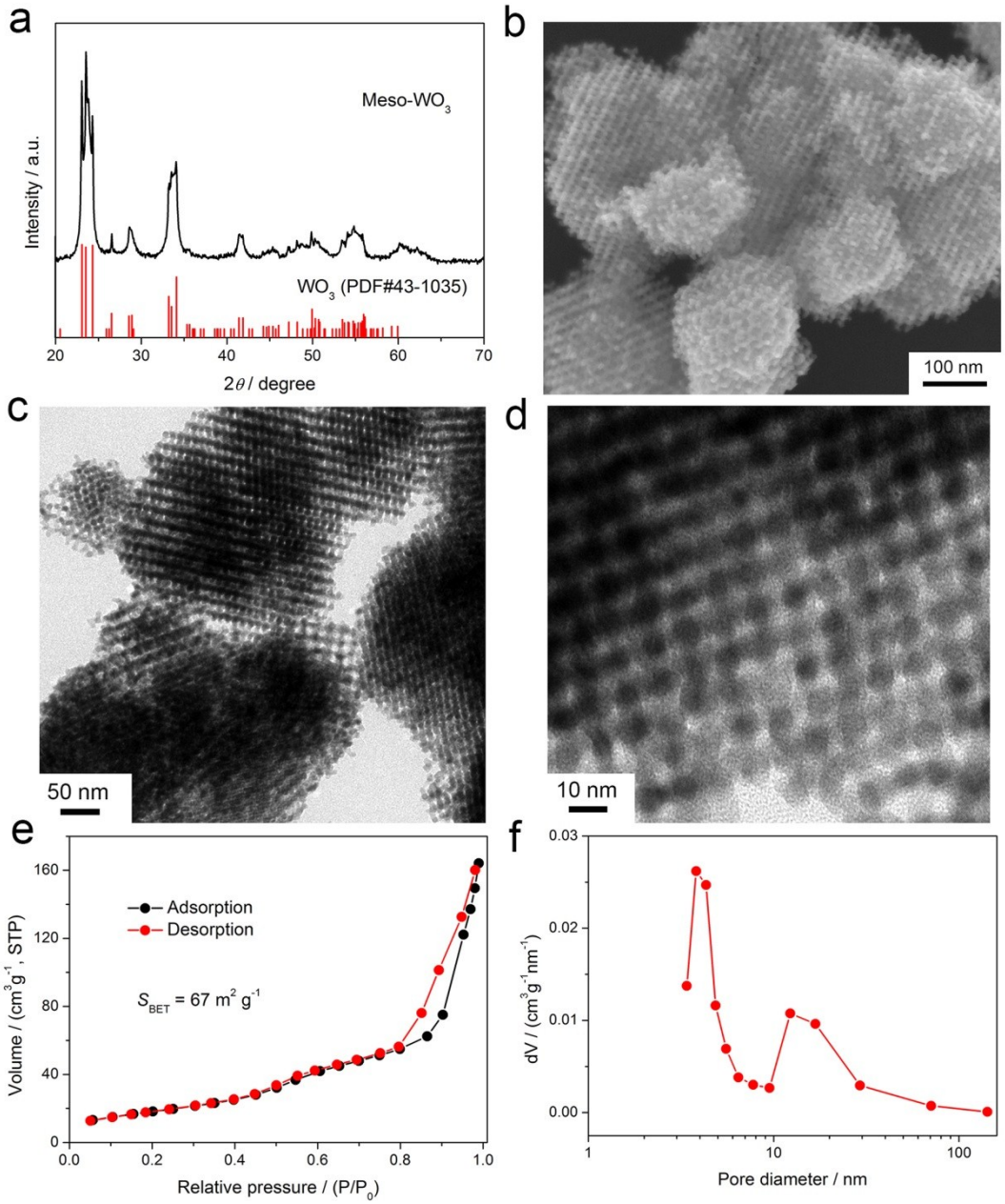


**Fig. S2** Structural characterizations of Meso-$WO_3$. (a) XRD pattern, (b) typical SEM image, (c,d) TEM images, (e) $N_2$ sorption isotherms and (f) the corresponding pore size distribution curves of the Meso-$WO_3$. The drop lines in (a) show the standard patterns of monoclinic $WO_3$ (red, PDF#43-1035). After impregnation with PTA precursors, calcination at 650 °C and removal of the KIT-6 template by $NH_4HF_2$, the as-prepared product is well assigned to monoclinic $WO_3$. SEM and TEM images further confirmed the ordered mesoporous structure of $WO_3$ product. The as-prepared Meso-$WO_3$ has a specific surface area of 67 $m^2/g$ and bi-model size distributions.

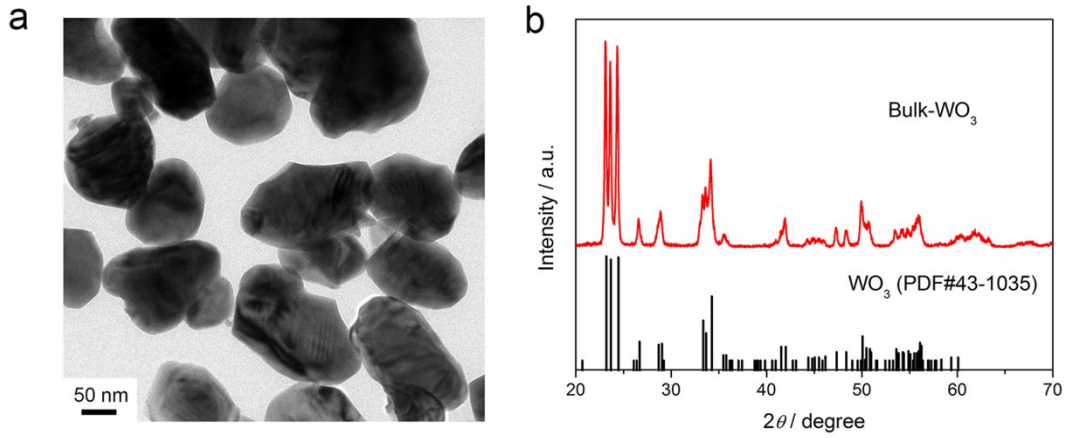


**Fig. S3** (a) TEM image of the commercial bulk $WO_3$ material. (b) XRD pattern of the commercial bulk $WO_3$. The drop line shows the standard XRD pattern of monoclinic $WO_3$ (PDF#43-1035). With particle size ranging from one hundred to several hundreds of nanometers, Bulk-$WO_3$ has a specific area of 4.6 $m^2/g$.

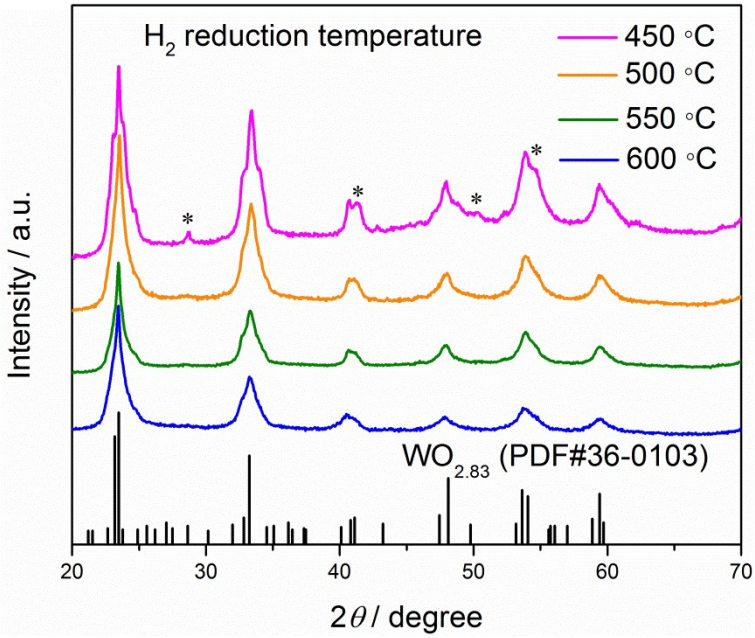


**Fig. S4** XRD patterns of the products through $H_2$ reduction of mesoporous $WO_3$ at 450, 500, 550 and 600 °C, respectively. The drop lines indicate the standard XRD patterns of monoclinic $WO_{2.83}$ and the asterisks (*) present the XRD peaks from monoclinic $WO_3$. It is seen that the products by $H_2$ reduction of Meso-$WO_3$ at 500, 550 and 600 °C are well assigned to $WO_{2.83}$, while partial $WO_3$ still remains in the product by $H_2$ reduction of Meso-$WO_3$ at 450 °C.

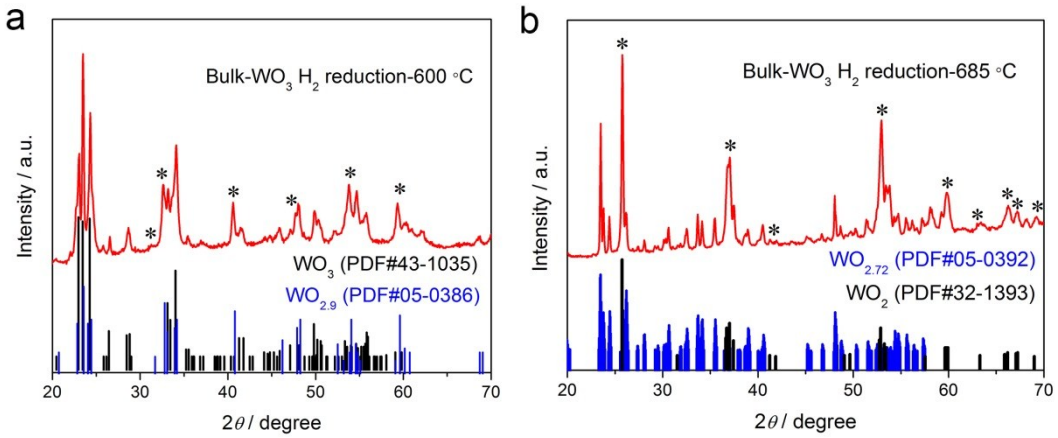


**Fig. S5** (a) XRD pattern of the commercial bulk $WO_3$ after $H_2$ reduction at 600 °C for 1 h. The drop line shows the standard XRD pattern of monoclinic $WO_3$ (PDF#43-1035) and $WO_{2.9}$ (PDF#05-0386), and the XRD peaks marked with asterisks (*) are attributed to $WO_{2.9}$. (b) XRD pattern of the commercial bulk $WO_3$ after $H_2$ reduction at 685 °C for 1 h. The drop line shows the standard XRD pattern of monoclinic $WO_{2.72}$ (PDF#05-0392) and $WO_2$ (PDF#32-1393), and the XRD peaks marked with asterisks (*) are attributed to $WO_2$. The XRD patterns suggest that after $H_2$ reduction at 600 and 685 °C for 1h, $WO_{2.9}$ and $WO_{2.72}$ as the intermediate sub-stoichiometric $WO_{3-x}$ occur in the of Bulk-$WO_3$.

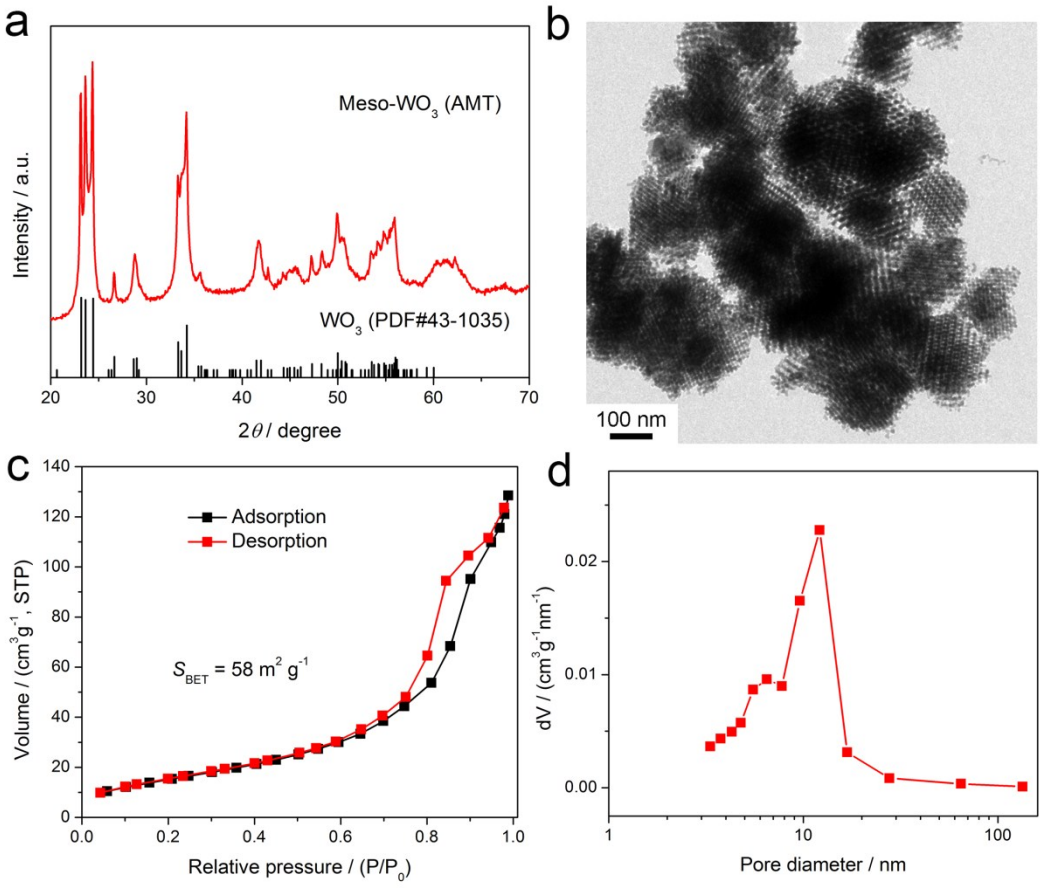


**Fig. S6** (a) XRD pattern, (b) TEM image, (c) $N_2$ sorption isotherm and (d) the corresponding pore size distribution curve of the Meso-$WO_3$ (AMT) product prepared by using ammonium metatungstate (AMT) as precursors. The drop lines in (a) indicate the standard XRD patterns of monoclinic $WO_3$ (black, PDF#43-1035).

As the derived Meso-$WO_3$ from phosphotungstic acid precursor contains 2.9 wt% of phosphorus (P) based on inductively coupled plasma optical emission spectrometry (ICP-OES), to exclude the possible influence of P element and verify the role of mesoporous structure in the phase engineering process, ammonium metatungstate (AMT) as a P-free precursor was also conducted to prepare Meso-$WO_3$ (Figure S6). With AMT as W precursor, mesoporous structure was also able to be prepared, which is well indexed to be monoclinic $WO_3$. The Meso-$WO_3$ (AMT) has a BET surface area of 58 $m^2/g$ and a dominant pore size of around 12 nm.

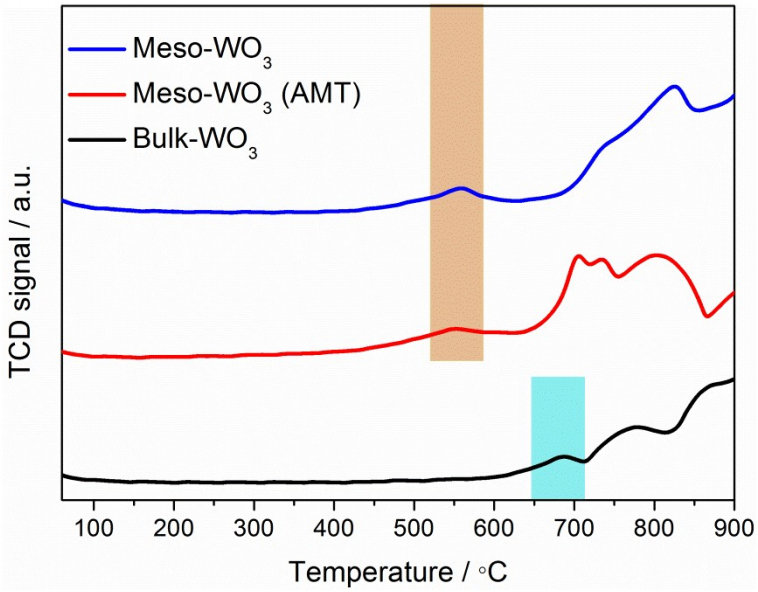


**Fig. S7** $H_2$ TPR plots of commercially available Bulk-$WO_3$ and as-prepared Meso-$WO_3$.

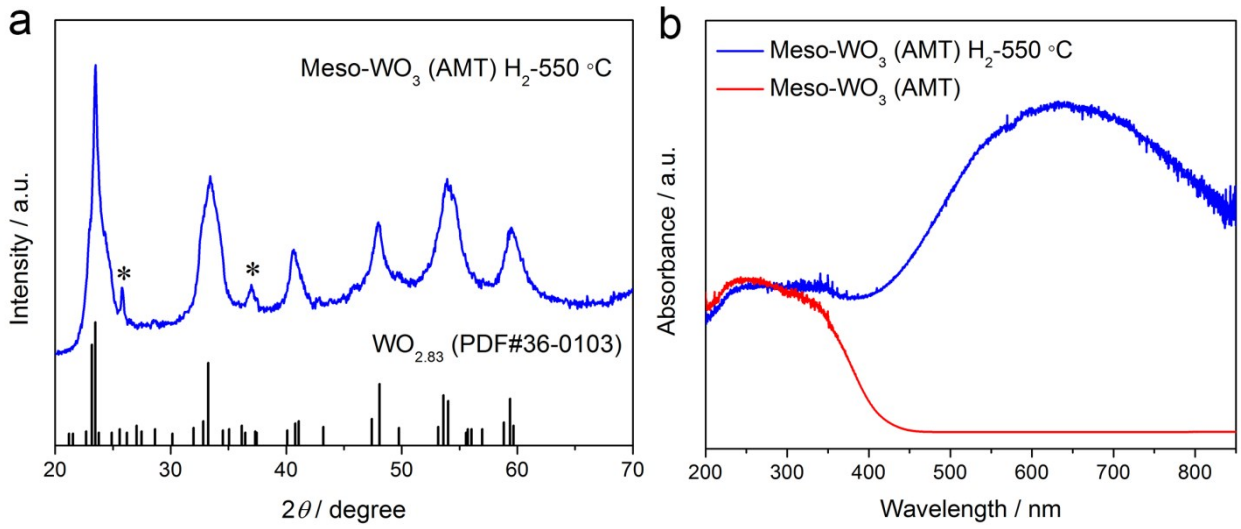


**Fig. S8** XRD pattern of the Meso-$WO_3$ (AMT) product after $H_2$ reduction at 550 °C. The drop lines in indicate the standard XRD patterns of monoclinic $WO_{2.83}$ (black), and the asterisks (*) present the XRD peaks from monoclinic $WO_2$. (b) UV/vis diffuse reflectance spectra of the Meso-$WO_3$ (AMT) products before and after $H_2$ reduction at 550 °C.Upon $H_2$ reduction at 550 °C, the as-prepared product mainly consists of monoclinic $WO_{2.83}$, and slight $WO_2$ was

formed due to over-reduction, which shows strong plasmonic resonance in the visible light region with absorption peak centering at 650 nm.

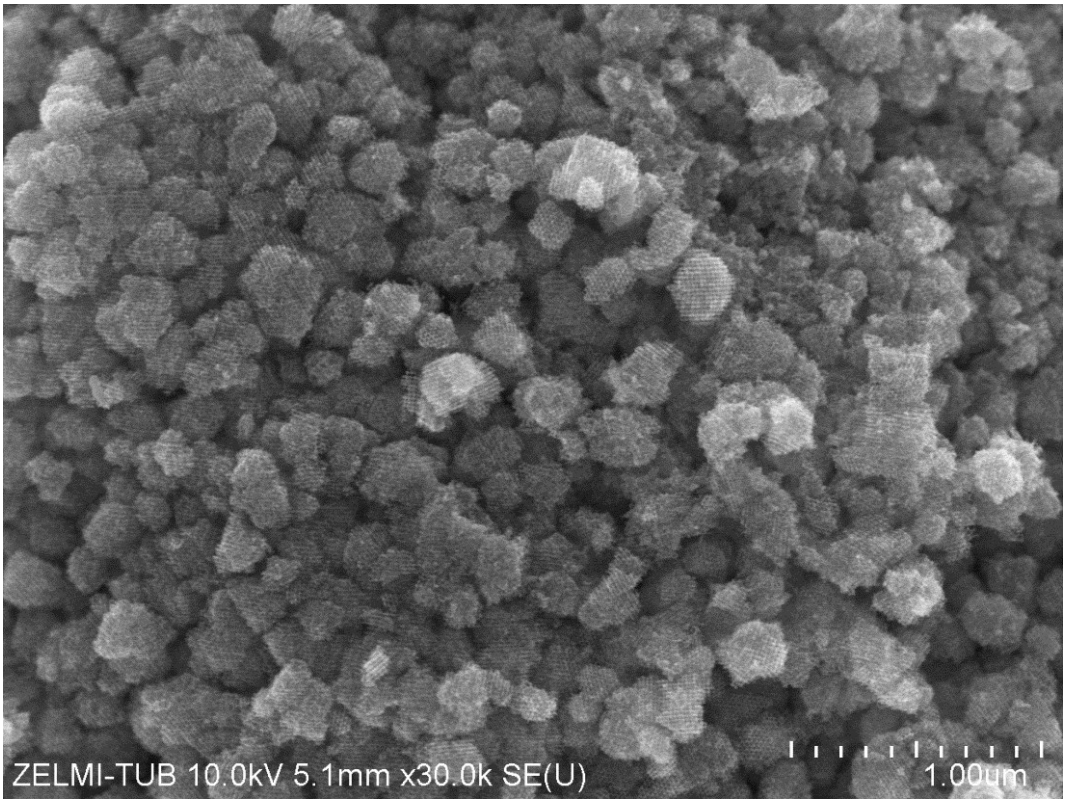


**Fig. S9** Large area SEM image of the as-prepared well-ordered mesoporous $WO_{2.83}$. The well-resolved stripes in the large-area SEM image show the uniformity of the well-ordered mesoporous $WO_{2.83}$.

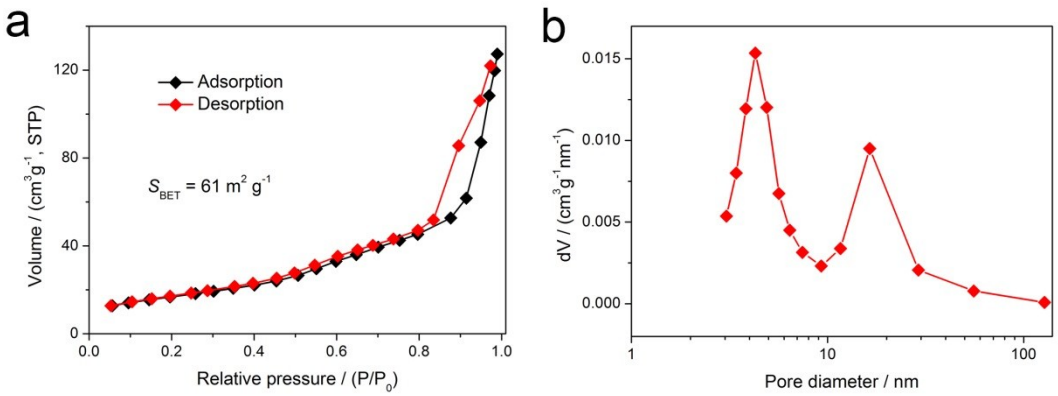


**Fig. S10 (**a) $N_2$ sorption isotherms and (b) the corresponding pore size distribution curves of the as-prepared Meso-$WO_{2.83}$ product.

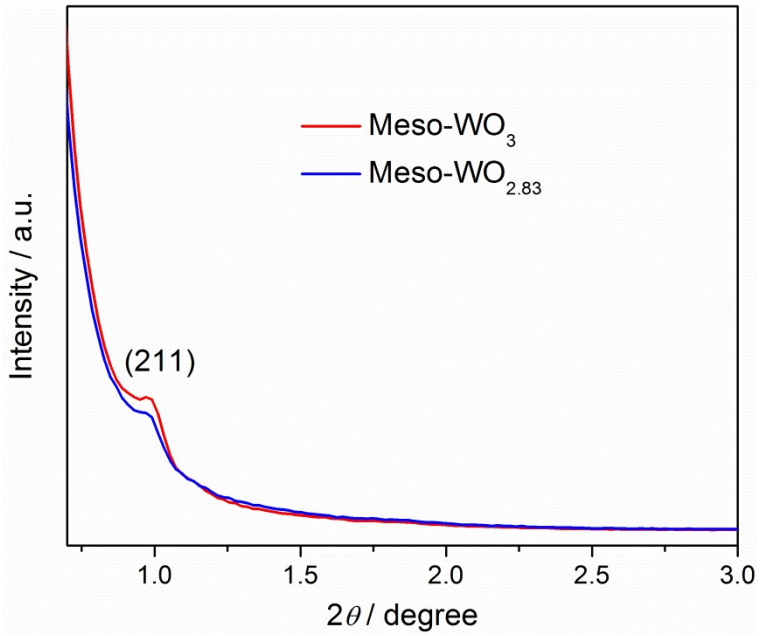


**Fig. S11** Small-angle XRD patterns of the Meso-$WO_3$ and Meso-$WO_{2.83}$ products.


**Fig. S12** Photographs of the (a) Meso-$WO_3$ and (b) Meso-$WO_{2.83}$ samples.

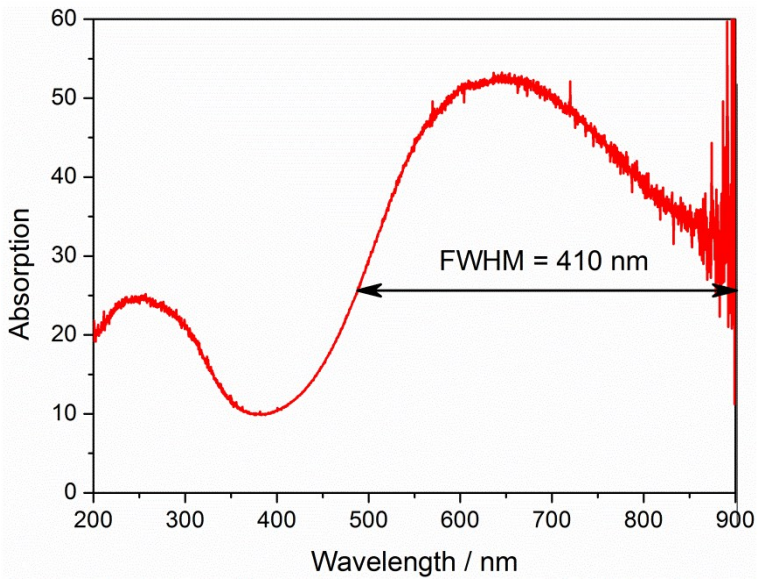


**Fig. S13** UV/vis diffuse reflectance spectrum of the Meso-$WO_{2.83}$ sample. The surface plasmon resonance peak is located at about 650 nm, with an approximate line width of 410 nm.

## Free carrier density calculations of plasmonic Meso-$WO_{2.83}$

The plasmonic resonance of Meso-$WO_{2.83}$ is related to the abundant delocalized electrons induced by oxygen vacancies, which could be described by the Drude model.[2] At the resonance condition, the plasmonic frequency $\omega_{sp}$ can be expressed as

$$\omega_{sp} = \sqrt{\frac{\omega_p^{\,2}}{1+2\varepsilon_m} - \gamma^2} \tag{1}$$

where $\omega_p$ is the bulk plasma, $\varepsilon_m$ is dielectric constant of the surrounding medium and $\gamma$ is the damping parameter that numerically equals to the linewidth of the plasmon resonance band.[3] In our case, the value of $\varepsilon_m$ is 1. For Meso-$WO_{2.83}$, the resonance energy equals to 1.91 eV at the plasmonic wavelength (650 nm), and the linewidth of 0.33 eV by measuring the full width at half-maximum (FWHM) of the optical spectrum (approximately 410 nm, Figure S13). Therefore, the bulk plasma frequency $\omega_p$ is approximately estimated to be 3.36 eV. Moreover, the bulk plasma frequency $\omega_p$ depends on the free electrons density $N$ by the formula

$$\omega_p^{\,2} = \frac{Ne^2}{\varepsilon_0 m^*} \tag{3}$$

where $e$ is the elementary charge, $\varepsilon_0$ is the permittivity of free space, and $m^*$ is the effective mass of the free carriers. According to the previous report,[4] the effective electron mass of $WO_{2.83}$ is set to be $m^* = 1.2m_0$, and $m_0$ is the electron rest mass. Therefore, the free electron concentration $N$ is estimated to be $9.79 \times 10^{21}$ $cm^{-3}$ in the Meso-$WO_{2.83}$ product.

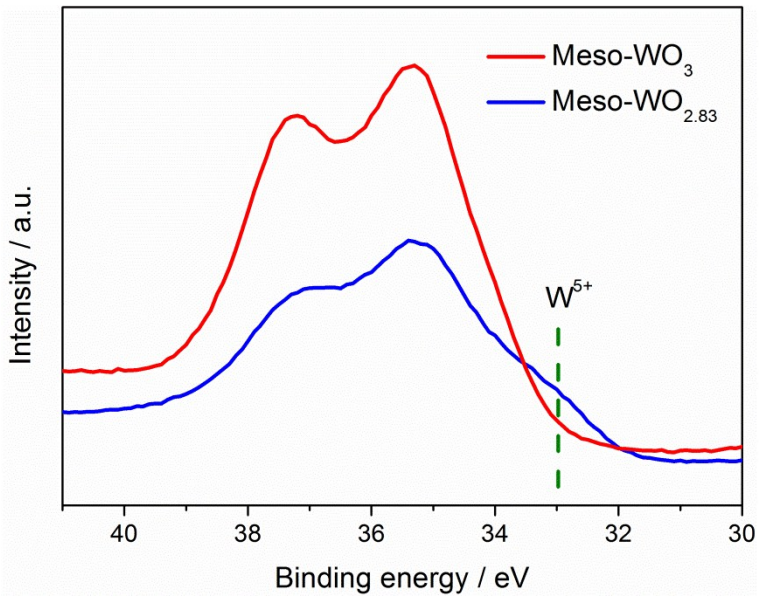


**Fig. S14** High-resolution W 4*f* XPS spectra of Meso-$WO_3$ and Meso-$WO_{2.83}$. The dashed line highlights the presence of $W^{5+}$ oxidation state locating at around 33 eV in Meso-$WO_{2.83}$, whereas this band disappears in pristine Meso-$WO_3$.

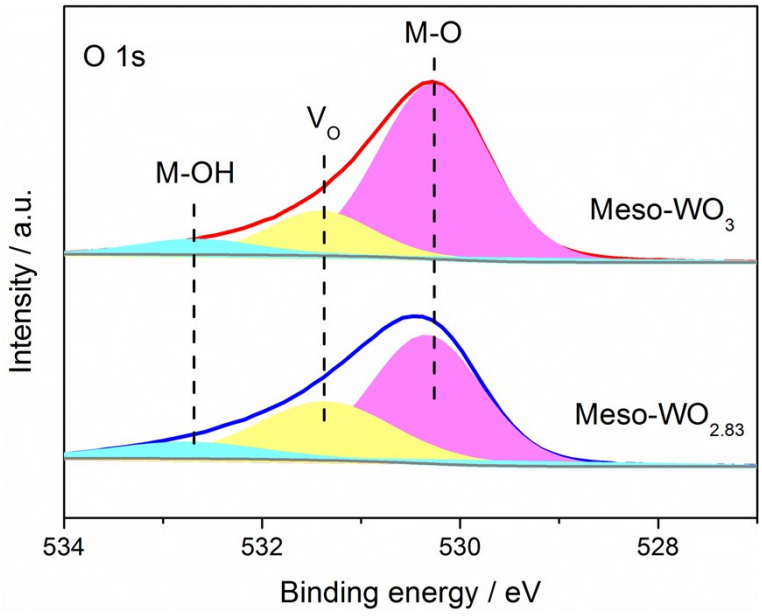


**Fig. S15** O 1s XPS spectra of the Meso-$WO_3$ and Meso-$WO_{2.83}$ products.

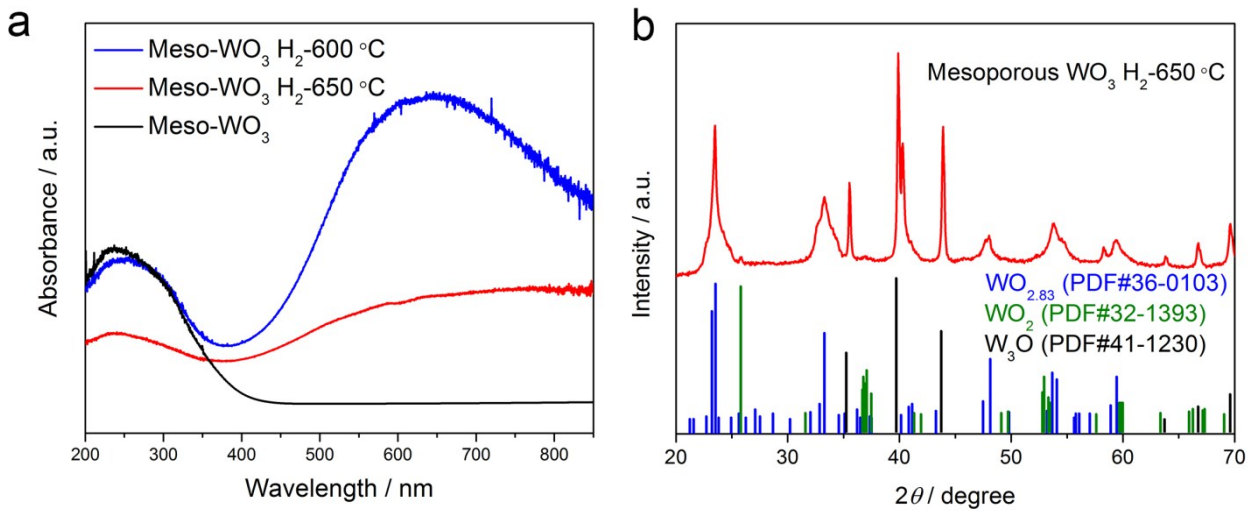


**Fig. S16** (a) UV/vis diffuse reflectance spectra of the mesoporous $WO_3$ products before and after $H_2$ reduction at 600 and 650 °C, respectively. (b) XRD pattern of the product by $H_2$ reduction of mesoporous $WO_3$ at 650 °C. The drop lines indicate the standard XRD patterns from monoclinic $WO_{2.83}$ (blue, PDF#36-0103), monoclinic $WO_2$ (olive, PDF#32-1393), and cubic $W_3O$ (black, PDF#41-1230).

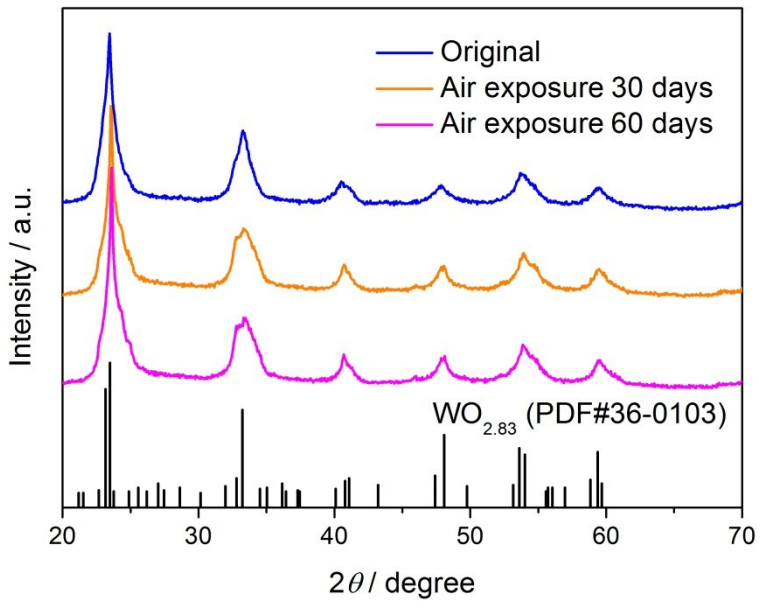


**Fig. S17** XRD patterns of the mesoporous $WO_{2.83}$ products upon air exposure for different time. The drop lines indicate the monoclinic $WO_{2.83}$ (PDF#36-0103).

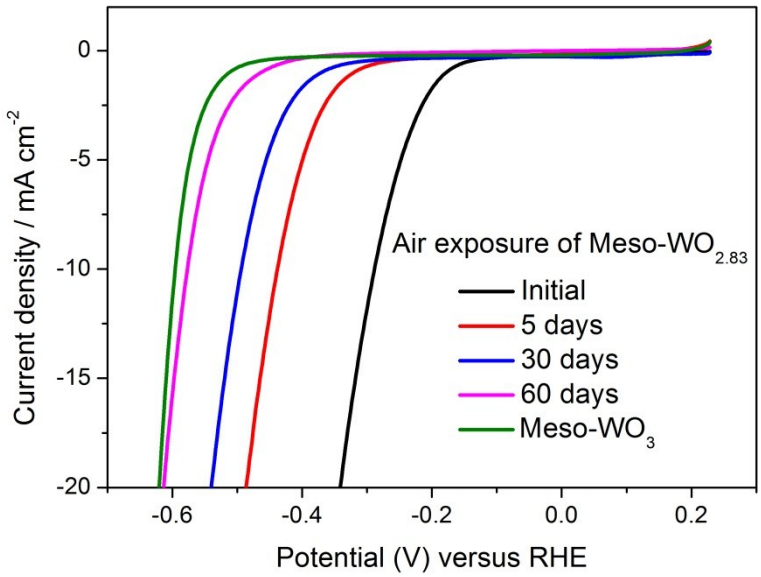


**Fig. S18** Polarization curves for electrocatalytic HER performances of Meso-$WO_{2.83}$ products upon air exposure for different time together with Meso-$WO_3$.

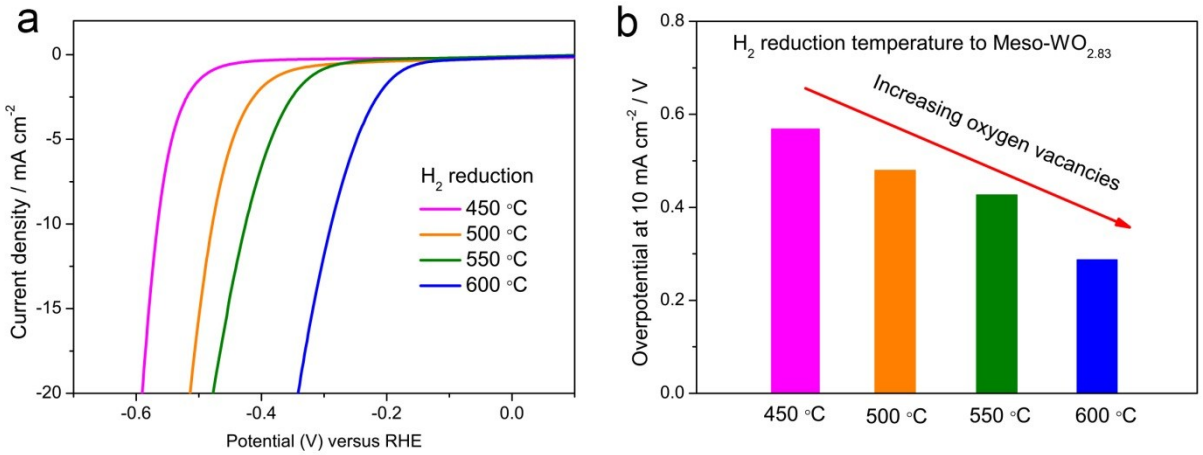


**Fig. S19** (a) Polarization curves for electrocatalytic HER performances of Meso-$WO_{2.83}$ products prepared at various $H_2$ reduction temperatures. (b) The overpotential comparison of Meso-$WO_{2.83}$ products prepared at various $H_2$ reduction temperatures at the current density of 10 mA $cm^{-2}$.

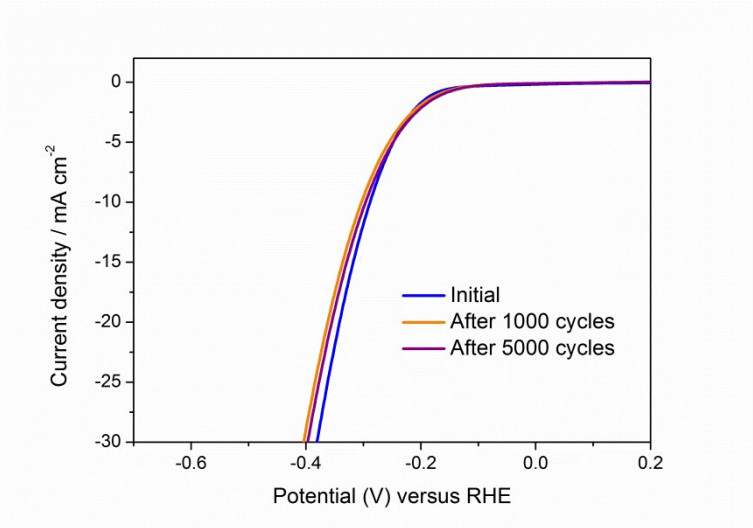


**Fig. S20** Polarization curves of Meso-$WO_{2.83}$ initially and after 1000 and 5000 CV scans.

**Table S1. Summary of some reported plasmonic doped-semiconductors.**

| Plasmonic Materials | Morphology | LSPR wavelength (nm) | Reference |
|---|---|---|---|
| **$WO_{2.83}$** | Mesoporous structure | 650 | This work |
| **$WO_{3-x}$** | Nanorods | ~900 | *J. Am. Chem. Soc.* **2012**, *134*, 3995 |
| **$WO_{3-x}$** | Nanosheets | 1450 | *Adv. Mater.* **2015**, *27*, 1580 |
| **$MoO_{3-x}$** | Nanosheets | 680 | *Angew. Chem. Int. Ed.* **2014**, *53*, 2910 |
| **$TiO_{2-x}$** | Nanocrystals | ~3400 | *J. Am. Chem. Soc.* **2012**, *134*, 6751 |
| **$Cu_{2-x}S$** | Quantum dots | 1800 | *Nat. Mater.* **2011**, *10*, 361 |
| **$Cu_{2-x}Se$** | Nanocrystals | 1100-1700 | *J. Am. Chem. Soc.* **2011**, *133*, 11175 |
| **$Cu_3P$** | Nanoplatelets | ~1800 | *Angew. Chem. Int. Ed.* **2013**, *52*, 6762. |
| **$Cu_xIn_yS_2$** | Quantum dots | ~1500 | *Nano Lett.* **2014**, *14*, 3262 |
| **GeTe** | Nanoparticles | ~2500 | *Phys. Rev. Lett.* **2013**, *111*, 037401 |
| **P-doped Si** | Nanocrystals | >2500 | *Nano Lett.* **2013**, *13*, 1317 |
| **In-doped $SnO_2$ (ITO)** | Nanoparticles | 1618−>2200 | *J. Am. Chem. Soc.* **2009**, *131*, 17736 |
| **Al-doped ZnO (AZO)** | Nanocrystals | >2500 | *Nano Lett.* **2011**, *11*, 4706 |

**Table S2. Summary of some reported $WO_{3-x}$-based electrocatalyst for HER.**

| Catalyst | $J$ (mA cm$^{-2}$) | $\eta_{10}$ (mV) | Ref. |
|---|---|---|---|
| **Meso-$WO_{2.83}$** | 10 | 288 | This work |
| **$W_{18}O_{49}$ nanofibers** | 10 | 425 | *Chem. Commun.* **2017**, *53*, 4323. |
| **$WO_{2.9}$** | 10 | 70 | *Nat. Commun.* **2015**, *6*, 8064. |
| **$W_{18}O_{49}/WS_2$** | 10 | 310 | *Chem. Commun.* **2015**, *51*, 8334 |
| **1%Pd-doped $W_{18}O_{49}$** | 10 | 331 | *Chem. Commun.* **2017**, *53*, 4323 |
| **$WO_{3-x}$/C (10%)** | 10 | 300 | *ACS Appl. Mater. Interfaces* **2016**, *8*, 18132. |
| **Ta-doped $WO_3$** | 10.72 | 520 | *Electrochim. Acta* **2014**, *134*, 201. |

## References


[1] F. Kleitz, S. H. Choi, R. Ryoo, *Chem. Commun.* **2003**, 2136.

[2] A. Comin, L. Manna, *Chem. Soc. Rev.* **2014**, *43*, 3957.

[3] F. Wang, F. Q. Li, L. Lin, H. Peng, Z. Liu, D. Xu, *J. Am. Chem. Soc.* **2015**, *137*, 12006.

[4] K. Manthiram, A. P. Alivisatos, *J. Am. Chem. Soc.* **2012**, *134*, 3995.